energies

MDPI

Article

Frequency-Controlled Current-Fed Resonant Converter with No Input Ripple Current

Bor-Ren Lin * and Guan-Hong Lin

Department of Electrical Engineering, National Yunlin University of Science and Technology, Yunlin 640, Taiwan; M10612096@yuntech.edu.tw

* Correspondence: linbr@yuntech.edu.tw; Tel.: +886-912312281

Received: 25 January 2018; Accepted: 9 February 2018; Published: 11 February 2018

Abstract: This paper studies a frequency-controlled current-fed resonant circuit. The adopted direct current (DC)-to-DC converter contains two boost circuits and a resonant circuit on the primary side. First, two boost circuits are connected in parallel to achieve voltage step-up and reduce input ripple current by using interleaved pulse-width modulation. Therefore, the size and current rating of boost inductors are decreased in the proposed converter. Second, the boost voltage is connected to the resonant circuit to realize the mechanism of the zero-voltage switching of all active switches and zero-current switching of all diodes. Two boost circuits and a resonant circuit use the same power devices in order to lessen the switch counts. The voltage doubler topology is adopted on the secondary side (high-voltage side). Therefore, the voltage rating of diodes on the high-voltage side is clamped at output voltage. The feasibility of the studied circuit is confirmed by the experimental tests with a 1 kW prototype circuit.

Keywords: current-fed resonant converter; frequency control; ripple current; boost converter

1. Introduction

Due to increased global warming and climbing temperature issues, renewable energy sources have been developed to produce clean energy. A fuel cell is a kind of renewable energy source that converts chemical energy to electric direct current (DC) or alternating current (AC) power. A solar cell is the other source of renewable energy to convert photovoltaic (PV) energy to electric DC or AC power. The outputs of fuel cell stacks and PV panels are low voltage. For connecting fuel cell stacks and PV panels to AC grids or DC grids [1,2], a voltage boost circuit and an isolation transformer are necessary. The high-voltage boost converters can be the voltage source type [3,4] or the current source type [5–7] circuit topologies. Normally, the input current ripple of the current source converters is much smaller than the voltage source converters. However, the main problems of high-voltage boost converters operating under high switching frequency are serious core losses and switching losses. Power converters with soft-switching turn-on or turn-off characteristics have been proposed and studied to overcome these problems. Duty cycle control [8–13] and frequency control schemes [14–16] are normally used to regulate load voltage and also reduce switching losses under zero-voltage or zero-current. The advantages of duty cycle control with fixed switching frequency are easy implementation with commercial integrated circuits and many available circuit topologies. However, the drawback of these topologies is poor circuit efficiency at low load, due to hard switching at low output power. Resonant converters [14–16] with frequency modulation have developed to achieve advantages of low switching losses at whole load range and high efficiency under low load conditions. Two boost converters and two full-bridge resonant converters with interleaved pulse-width modulation (PWM) are adopted in [5] to obtain high voltage gain and less input ripple current for electric vehicle (EV) and hybrid electric vehicle (HEV) applications. However, more power devices (10 power switches) are used in this circuit topology such that the cost is increased and the reliability is reduced.

This paper proposes and studies a simple voltage-boost current-fed resonant DC/DC circuit. The studied converter has two voltage boost circuits, a frequency-controlled full-bridge circuit and a voltage doubler rectifier. The voltage boost circuits and full-bridge circuit use the same active devices so that the total active devices are decreased. Interleaved PWM is adapted to control two voltage boost circuits. Due to the interleaved PWM operation with one-half cycle phase shift, the input current ripple of the proposed converter is reduced to zero. Since the full-bridge circuit is controlled by frequency modulation, the mechanism of the zero-voltage switching of all active switches and zero-current switching of all diodes can be realized at whole load range. Therefore, the turn-on switching losses of active switches and turn-off switching losses or the reverse recovery current losses of the diodes are decreased. A voltage doubler circuit topology is used on the secondary side (high-voltage side) in order to limit the voltage stress of diode at load voltage. In Section 2, the circuit diagram and structure of the studied circuit topology are presented and discussed. The circuit operation is presented in Section 3. The circuit performance and design examples are provided in Section 4. Finally, the feasibility of the developed circuit is verified by a 1 kW prototype circuit in Section 5, followed by the conclusions.

2. Proposed Converter

Figure 1a gives the circuit schematic of the studied converter. V_{in} is input voltage, V_o is output voltage, Q_1~Q_4 are active switches, L_{b1} and L_{b2} are boost inductors, C_b is boost capacitor, C_r and L_r are resonant capacitor and inductor, T is an isolation transformer, D_1 and D_2 are fast recovery diodes, and C_{o1} and C_{o2} are output capacitors. On the secondary side (high-voltage side), a voltage doubler rectifier is employed to limit the voltage rating of fast recovery diodes for high voltage output applications. The proposed circuit includes two interleaved boost converters (V_{in}, Q_1~Q_4, L_{b1}, L_{b2} and C_b) and a full-bridge resonant converter (C_b, Q_1~Q_4, L_r, C_r, T, D_1, D_2, C_{o1} and C_{o2}) to achieve high voltage gain, no input ripple current and soft switching of active switches. In Figure 1b, two voltage boost converters are operated by using interleaved PWM to achieve voltage step-up. Since the duty cycle of each of the active switches Q_1~Q_4 is 0.5, it can obtain $V_b = 2\ V_{in}$. Since the gated signals of two voltage boost converters are phase-shifted by one-half of the switching period, the boost inductor ripple currents Δi_{Lb1} and Δi_{Lb1} are cancelled each other so that the input ripple current $\Delta i_{in} = \Delta i_{Lb1} + \Delta i_{Lb2} = 0$. Therefore, no ripple current ($\Delta i_{in} = 0$) is realized at input side. In Figure 1c, the full-bridge resonant circuit is operated by frequency control to produce a nearly sinusoidal current and voltage on the resonant tank by L_r, C_r and L_m. Due to the resonant tank of the full-bridge circuit being worked at inductive load, the zero-voltage switching of Q_1~Q_4 is realized at the whole load. Frequency modulation is used to control load voltage. The studied converter can be used in a battery charger/discharger with switches on the high-voltage terminal in the proposed converter and low-voltage input renewable energy source such as solar cell panel.

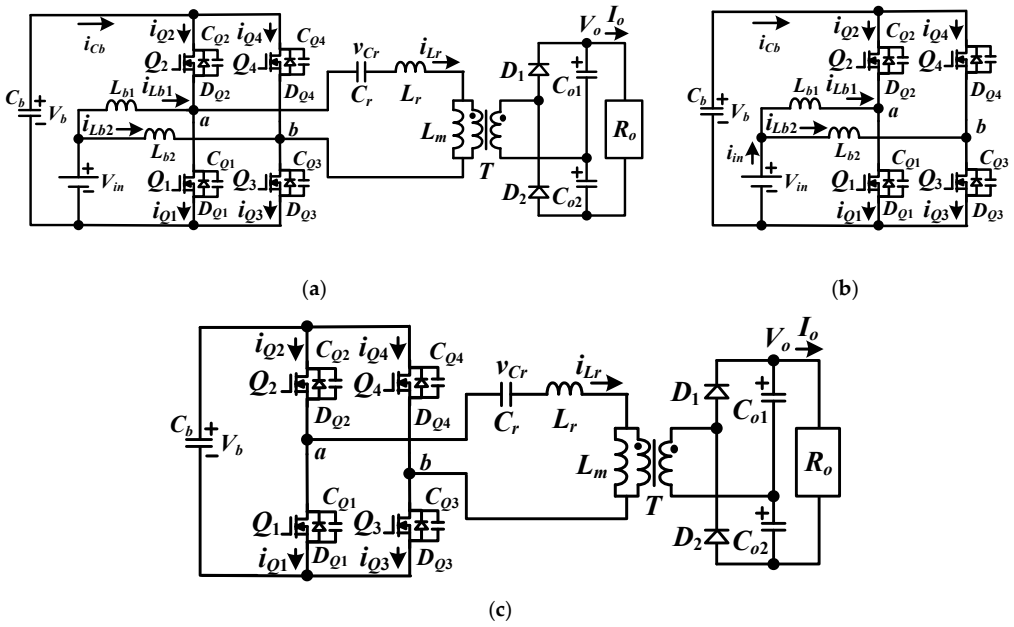

Figure 1. Proposed converter (**a**) circuit diagram (**b**) boost converter operation (**c**) full-bridge resonant converter operation.

3. Circuit Operation

Two boost circuits with interleaved PWM schemes are connected in parallel to decrease the current stress of active devices and to obtain no input ripple current. Since Q_1~Q_4 all have 0.5 duty cycles, it can obtain the boost voltage $V_b = 2\ V_{in}$. The full-bridge resonant circuit is operated at inductive load with frequency control. Therefore, Q_1~Q_4 have zero-voltage switching with low switching loss, and D_1 and D_2 have zero-current switching with no reverse recovery current loss. The studied converter is assumed $L_{b1} = L_{b2} = L_b$, $C_{Q1} = C_{Q2} = C_{Q3} = C_{Q4} = C_Q$, $C_{o1} = C_{o2}$ and $V_{o1} = V_{o2} = V_o/2$. Figure 2 gives the PWM waveforms of the studied circuit at a switching cycle. Based on the switching states of D_1, D_2 and Q_1~Q_4, the studied converter can be divided into six operating steps in each switching period when the series resonant frequency is more than the switching frequency. Figure 3 gives these six equivalent circuits. Before step 1, Q_1~Q_4 are off, D_2 conducts, $i_{Lb1} > 0$, $i_{Lb2} > 0$ and $i_{Lr} > 0$.

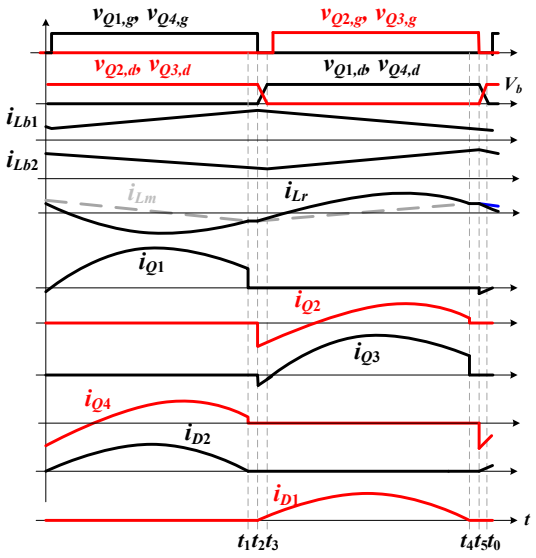

Figure 2. PWM waveforms of the developed circuit.

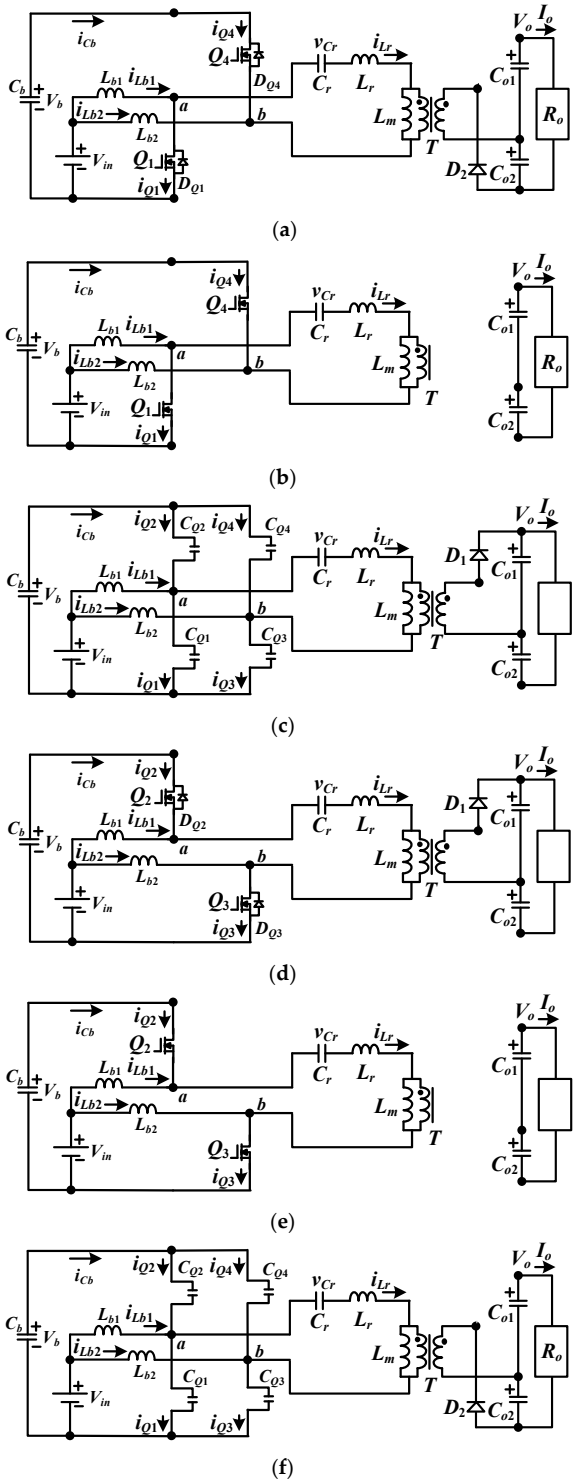

Figure 3. Six equivalent circuits in a switching period (**a**) operating step 1 (**b**) operating step 2 (**c**) operating step 3 (**d**) operating step 4 (**e**) operating step 5 (**f**) operating step 6.

Step 1 [t_0~t_1]: At time t_0, capacitors C_{Q1} and C_{Q4} are discharged to zero voltage. Since $i_{Lb1} - i_{Lr} < 0$ and $i_{Lr} + i_{Lb2} > 0$, the body diodes D_{Q1} and D_{Q4} are forward biased. At this time instant, switches Q_1 and Q_4 are turned on under zero-voltage switching. Since Q_1 and Q_4 are turned on in this step, v_a =

0 and $v_b = V_b$. The boost inductor voltages $v_{Lb1} = V_{in}$ and $v_{Lb2} = V_{in} - V_b$. Since $V_b > V_{in}$, i_{Lb1} increases linearly and i_{Lb2} decreases linearly.

$$\frac{di_{Lb1}}{dt} = \frac{V_{in}}{L_b}, \frac{di_{Lb2}}{dt} = \frac{V_{in} - V_b}{L_b} \tag{1}$$

For the full-bridge resonant converter, energy is transferred from C_b to the secondary side (high-voltage side) through a resonant tank with L_r and C_r. Since D_2 is forward biased, the primary winding voltage $v_{Lm} = -V_o/2$, the current of L_m, i_{Lm}, decreases linearly with $-nV_o/(2L_m)$ and C_{o2} is charged from the secondary current of transformer T. In this step, L_r and C_r are resonant with $f_r = 1/2\pi\sqrt{L_rC_r}$. The solutions of primary side current and voltage are given as

$$i_{Lr}(t) = \frac{[\frac{nV_o}{2} - 2V_{in} - v_{Cr}(t_0)]}{\sqrt{L_r/C_r}} \sin\frac{t - t_0}{\sqrt{L_rC_r}} + i_{Lr}(t_0)\cos\frac{t - t_0}{\sqrt{L_rC_r}} \tag{2}$$

$$v_{Cr}(t) = i_{Lr}(t_0)\sqrt{L_r/C_r}\sin\frac{t - t_0}{\sqrt{L_rC_r}} + \frac{nV_o}{2} - 2V_{in} - [\frac{nV_o}{2} - 2V_{in} - v_{Cr}(t_0)]\cos\frac{t - t_0}{\sqrt{L_rC_r}} \tag{3}$$

where $n = n_p/n_s$. If the series resonant frequency f_r is more than the switching frequency f_{sw}, then the secondary side current of transformer T decreases to zero current at time t_1 and the circuit operation goes to step 2. Otherwise, the circuit operation will go to step 3 under $f_{sw} > f_r$ condition.

Step 2 [t_1~t_2]: i_{D2} decreases to zero current at time t_1 and D_2 becomes reverse biased. In this step, i_{Lb1} increases linearly, i_{Lb2} decreases linearly and i_{Lr} freewheels through Q_1 and Q_4. In this step, L_r, L_m and C_r are resonant with $\omega_p = 1/\sqrt{(L_r + L_m)C_r}$. The solutions of primary current i_{Lr} and resonant capacitor voltage v_{Cr} in this freewheeling state are given in (4) and (5).

$$i_{Lr}(t) = -\frac{[2V_{in} + v_{Cr}(t_1)]}{\sqrt{(L_r + L_m)/C_r}}\sin\frac{t - t_1}{\sqrt{(L_r + L_m)C_r}} + i_{Lr}(t_1)\cos\frac{t - t_1}{\sqrt{(L_r + L_m)C_r}} \tag{4}$$

$$v_{Cr}(t) = -2V_{in} + [2V_{in} + v_{Cr}(t_1)]\cos\frac{t - t_1}{\sqrt{(L_r + L_m)C_r}} + i_{Lr}(t_1)\sqrt{(L_r + L_m)/C_r}\sin\frac{t - t_1}{\sqrt{(L_r + L_m)C_r}} \tag{5}$$

Step 3 [t_2~t_3]: Q_1 and Q_4 are turned off at time t_2 under zero voltage. Since $i_{Lb1} - i_{Lr} > 0$ and $i_{Lr} + i_{Lb2} < 0$, C_{Q2} and C_{Q3} are discharged linearly.

$$\frac{dv_{CQ2}}{dt} = -\frac{i_{Lb1} - i_{Lr}}{2C_Q}, \frac{dv_{CQ3}}{dt} = \frac{i_{Lr} + i_{Lb2}}{2C_Q} \tag{6}$$

In this step, D_1 is forward biased and the primary winding voltages v_{Lm} is clamped at $nV_o/2$. The discharge time of C_{Q2} and C_{Q3} is soon enough so that i_{Lb1}, i_{Lb2} and i_{Lr} are almost constant during this step.

Step 4 [t_3~t_4]: The voltages on C_{Q2} and C_{Q3} are decreased to zero voltage at time t_3. Since $i_{Lb1} - i_{Lr} > 0$ and $i_{Lr} + i_{Lb2} < 0$, D_{Q1} and D_{Q4} are forward biased. Therefore, Q_2 and Q_3 can be turned on after t_3 and the zero-voltage switching of Q_2 and Q_3 is achieved. In this step, $v_a = V_b$ and $v_b = 0$ so that $v_{Lb1} = V_{in} - V_b$ and $v_{Lb2} = V_{in}$. Therefore, i_{Lb1} decreases linearly and i_{Lb2} increases linearly.

$$\frac{di_{Lb1}}{dt} = \frac{V_{in} - V_b}{L_b}, \frac{di_{Lb2}}{dt} = \frac{V_{in}}{L_b} \tag{7}$$

The energy is transferred from C_b to C_{o1} through L_r and C_r. Since D_1 is forward biased, the primary winding voltage $v_{Lm} = V_o/2$, i_{Lm} increases linearly and C_{o1} is charged. If the series resonant frequency f_r is more than the switching frequency f_{sw}, then the diode current i_{D1} will decrease to zero at time t_4 and circuit goes to step 5. On the other hand, the circuit will go to step 6 under the $f_{sw} > f_r$ condition.

Step 5 [t_4~t_5]: i_{D1} decreases to zero current at t_4 and D_1 becomes reverse biased. During step 5, i_{Lb1} decreases, i_{Lb2} increases and i_{Lr} freewheels through Q_2 and Q_3. C_r, L_r and L_m are resonant in step 5.

Step 6 [t_5~t_0]: At time t_5, Q_2 and Q_3 turn off under zero voltage. Since $i_{Lb1} - i_{Lr} < 0$ and $i_{Lr} + i_{Lb2} > 0$, C_{Q1} and C_{Q4} are discharged linearly.

$$\frac{dv_{CQ1}}{dt} = \frac{i_{Lb1} - i_{Lr}}{2C_Q}, \frac{dv_{CQ4}}{dt} = -\frac{i_{Lr} + i_{Lb2}}{2C_Q} \tag{8}$$

Rectifier diode D_2 is forward biased and $v_{Lm} = -nV_o/2$. Since the discharge time of C_{Q1} and C_{Q4} in step 6 is very soon, i_{Lb1}, i_{Lb2} and i_{Lr} are almost constant in this time interval.

4. Circuit Characteristics

4.1. Boost Converter

Two interleaved voltage boost circuits are worked in continuous conduction mode under the following assumptions: (1) power devices are ideal; and (2) inductors and capacitors are linear and time-invariant. Since the average value of the voltages across L_{b1} and L_{b2} is zero, it is possible to calculate the following equation based on the flux balance on the boost inductors.

$$V_b = V_{in}/(1 - D) \tag{9}$$

where D is a duty ratio of Q_1 and Q_4. Since D is fixed at 0.5 in the studied circuit, it can be calculated as $V_b = 2V_{in}$ and the DC voltage transfer function of boost converter is given as $M_{V.\,boost} = V_o/V_{in} = 2$. The PWM waveforms of Q_1 and Q_3 are phase shifted by $T_{sw}/2$. The ripple currents, Δi_{Lb1} and Δi_{Lb1}, on two boost inductors L_{b1} and L_{b2} are cancelled each other which gives $\Delta i_{in} = \Delta i_{Lb1} + \Delta i_{Lb2} = 0$. Thus, there is no ripple current ($\Delta i_{in} = 0$) from input voltage. The voltage ratings of Q_1~Q_4 are equal to V_b (=2 V_{in}). The average inductor currents I_{Lb1} and I_{Lb2} equal to $P_o/(2\ V_{in})$.

4.2. Full-Bridge Resonant Converter

The full-bridge resonant circuit includes two switching legs to draw two current pulses per switching cycle from the input voltage terminal and to deliver more output power than the half-bridge resonant circuit. To obtain advantages of the good light load efficiency of the series resonant circuit and the ability to control load voltage at light or open load of the parallel resonant circuit, the full-bridge *LLC* resonant circuit is employed in the studied circuit topology. Fundamental harmonic analysis from Steigerwald's article [17] is used to obtain the AC gain characteristics. Due to the PWM waveforms of Q_1~Q_4, the voltage v_{ab} is a square waveform with two voltage levels, V_b (=2 V_{in}) and $-V_b$ (=$-$2 V_{in}). Thus, the fundamental frequency voltage $v_{ab,f}$ is expressed as

$$v_{ab,f} = (8V_{in}/\pi)\sin(2\pi f_{sw}t) \tag{10}$$

Due the on-off states of D_1 and D_2, the transformer primary voltage v_{Lm} is a square waveform and the fundamental magnetizing voltage is given as

$$v_{Lm,f} = \frac{2nV_o}{\pi}\sin(2\pi f_{sw}t - \theta) \tag{11}$$

The fundamental secondary current of transformer is derived as

$$i_{s,T} = \pi I_o \sin(2\pi f_{sw}t - \theta) \tag{12}$$

Based on (11) and (12), R_{ac} is obtained from the secondary load R_o reflected into the primary side.

$$R_{ac} = \frac{v_{Lm,f}}{i_{s,T}/n} = \frac{2n^2}{\pi^2} R_o \tag{13}$$

Figure 4 gives the AC equivalent circuit of the adopted resonant circuit. $v_{ab,f}$ is an effectively sinusoidal input voltage and R_{ac} is an effective load. Therefore, the gain characteristics of the studied resonant circuit under different switching frequencies is calculated as

$$G_{ac}(f_{sw}) = \frac{\frac{R_{ac} \times j\omega_{sw} L_m}{R_{ac} + j\omega_{sw} L_m}}{j\omega_{sw} L_r - \frac{j}{\omega_{sw} C_r} + \frac{R_{ac} \times j\omega_{sw} L_m}{R_{ac} + j\omega_{sw} L_m}} = \frac{1}{1 + K(1 - \frac{1}{F^2}) + jQ(F - \frac{1}{F})} \tag{14}$$

where f_{sw} is the switching frequency, $f_r = 1/2\pi\sqrt{L_r C_r}$, $F = f_{sw}/f_r$, $K = L_r/L_m$ and $Q = \sqrt{L_r/C_r}/R_{ac}$. The amplitude of the AC gain from (14) can be further expressed as

$$|G_{ac}(f_{sw})| = \frac{1}{\sqrt{\left[1 + K(1 - \frac{1}{F^2})\right]^2 + Q^2(F - \frac{1}{F})^2}} \tag{15}$$

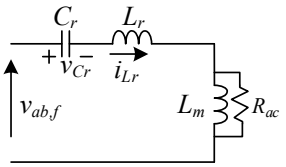

Figure 4. AC equivalent circuit of the full-bridge resonant circuit.

4.3. Design Procedure of the Developed Converter

A 1000 W prototype is set up to investigate the main circuit parameter design considerations. The electrical specifications of the developed converter are input voltage V_{in} = 44~52 V, output voltage V_o = 400 V, output power P_o = 1000 W, and the series resonant frequency f_r = 100 kHz. First, the boost converter with interleaved PWM is used to boost input voltage and reduce input ripple current. The duty cycle of Q_1~Q_4 is fixed at 0.5 with frequency modulation. The ripple currents Δi_{Lb1} and Δi_{Lb2} are calculated as

$$\Delta i_{Lo1} = \Delta i_{Lo2} = \frac{V_{in} T_{sw}}{2L_b} \tag{16}$$

Since the gate signals of Q_1 and Q_3 are phase shifted by $T_{sw}/2$ and each duty cycle of switches is equal to 0.5, it is obvious that the current ripple on the input side is decreased significantly and equals zero. The adopted boost inductors L_{b1} and L_{b2} are 37 μH. That means that the ripple currents on L_{b1} and L_{b2} at maximum input voltage and series resonant frequency are

$$\Delta i_{Lo1} = \Delta i_{Lo2} = \frac{V_{in} T_{sw}}{2L_b} = \frac{52 \times 10^{-5}}{2 \times 37 \times 10^{-6}} \approx 7\,\text{A} \tag{17}$$

In order to make sure the output voltage can be regulated at all input voltage ranges, the minimum DC voltage gain $G_{dc,\min}$ under $V_{Cb,\max}$ input is designed as unity. Thus, the turn-ratio is obtained in (18).

$$n = \frac{G_{dc,\min} V_{Cb,\max}}{V_o/2} = \frac{1 \times 52 \times 2}{400/2} = 0.52 \tag{18}$$

Transformer T is implemented by ferrite core TDK PC40 EER-42 with n_p = 13 and n_s = 25. Then, the theoretical maximum DC voltage gain under minimum input voltage is given as

$$G_{dc,\max} = \frac{nV_o}{2V_{Cb,\min}} = \frac{0.52 \times 400}{2 \times 44 \times 2} = 1.18 \tag{19}$$

Based on (13), R_{ac} under full load conditions can be calculated as

$$R_{ac} = \frac{2n^2}{\pi^2} R_o = \frac{2 \times 0.52^2}{3.1416^2} \times \frac{400^2}{1000} \approx 8.77\,\Omega \tag{20}$$

The inductor ratio $K = L_r/L_m$ will affect the circulating current loss on the primary side of the resonant converter. The lower inductor ratio K can reduce the circulating current loss due to larger L_m. However, the AC gain of resonant converter is reduced. The higher inductor ratio K can obtain larger AC voltage gain. However, the circulating current loss is increased to reduce circuit efficiency. Therefore, the selection K is a compromise between the AC voltage gain and the circulating current loss. Normally, the K is selected between 0.08–0.5. Considering these factors, the inductor ratio and quality factor are designed as $K = L_r/L_m = 1/6$ and $Q = 0.3$. Therefore, L_r and C_r are calculated as

$$L_r = \frac{QR_{ac}}{2\pi f_r} = \frac{0.3 \times 8.77}{2\pi \times 100{,}000} \approx 4.18\,\mu\text{H} \tag{21}$$

$$C_r = \frac{1}{4\pi^2 L_r f_r^2} = \frac{1}{4\pi^2 \times 4.18 \times 10^{-6} \times (100{,}000)^2} \approx 606\,\text{nF} \tag{22}$$

Considering the practical value of C_r, a 600 nF film capacitor is used for C_r. In a similar way, the resonant inductor L_r is actually selected as 4.22 μH. Since the inductor ratio $K = L_r/L_m = 1/6$ is adopted, the magnetizing inductance L_m is calculated as

$$L_m = L_r/k = \frac{4.22\,\mu\text{H}}{1/6} \approx 25.32\,\mu\text{H} \tag{23}$$

The voltage stress and average current of fast recovery diodes D_1 and D_2 are calculated in (24) and (25).

$$v_{D1,stress} = v_{D1,stress} \approx V_o = 400\,\text{V} \tag{24}$$

$$i_{D1,av} = i_{D2,av} = I_o = 2.5\,\text{A} \tag{25}$$

Diodes OM5262SW with 1000 V voltage rating and 12 A average current rating are adopted for D_1 and D_2. The voltage rating of Q_1~Q_4 are 2 × 52 V = 104 V. The MOSFETs IRFB52N15D with 150 V voltage rating and 60 A current rating are adopted for Q_1~Q_4. The 1100 μF capacitor is used for C_b and the 360 μF capacitors are used for C_{o1} and C_{o2}.

5. Experimental Results

The developed converter is implemented by a 1 kW prototype to demonstrate the circuit performance and verify the feasibility and effectiveness of the studied circuit. Figure 5 gives the experimental circuit diagram of the developed circuit. The photocoupler PC817 and voltage regulator TL431 are adopted to control load voltage. The resonant mode control integrated circuit UCC25600 is used to realize frequency modulation and achieve zero-voltage switching. The circuit parameters of active and passive components of the developed circuit are discussed and obtained from the previous section. From the experimental results in Figures 6–12, the test and experimental results agree with the PWM waveforms in Figure 2. The experimental results of the gate voltages of Q_1~Q_4 at rated power are illustrated in Figure 6. It can be observed that Q_1 (Q_2) and Q_3 (Q_4) have complementary PWM waveforms. The switching frequency of Q_1 at 44 V input is less than the switching frequency at 52 V input so that the resonant circuit can obtain larger voltage gain to regulate load voltage. The experimental waveforms of input current and boost inductor currents at the rated power are given in Figure 7. It can be observed that i_{Lb1} and i_{Lb2} are interleaved with each other and balanced well. The PWM waveforms of two boost circuits are interleaved by a phase shift of $T_{sw}/2$ so that the input ripple current Δi_{in} is reduced almost to zero.

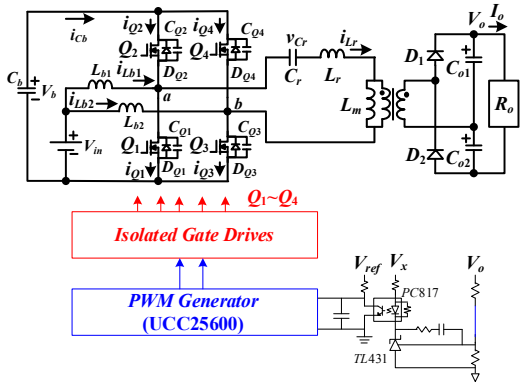

Figure 5. The prototype circuit diagram of the studied circuit.

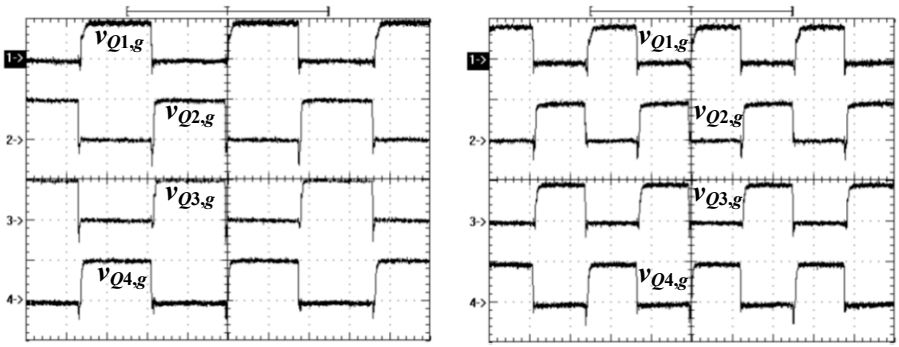

(**a**) (**b**)

Figure 6. Experimental results of the gating signals of Q_1~Q_4 under the rated power and (**a**) V_{in} = 44 V (**b**) V_{in} = 52 V [$v_{Q1,g}$~$v_{Q4,g}$: 10 V/div; time: 4 µs/div].

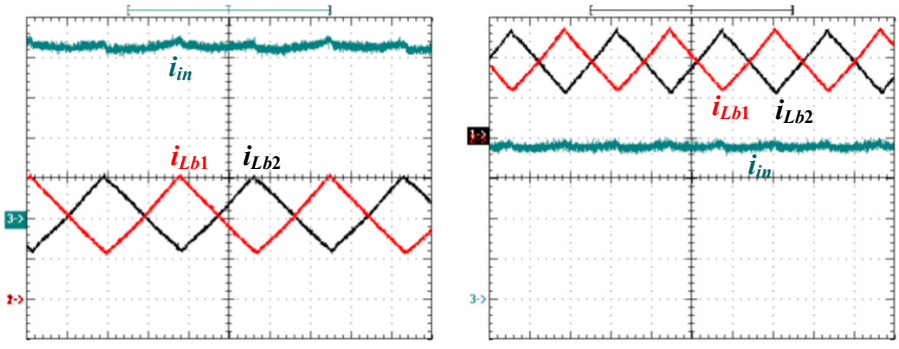

(**a**) (**b**)

Figure 7. Experimental results of input current and boost currents under the rated power and (**a**) V_{in} = 44 V (**b**) V_{in} = 52 V [i_{in}, i_{Lb1}, i_{Lb2}: 5 A/div; time: 4 µs/div].

The test results of boost voltage V_b, boost current i_{Cb} and switch currents i_{Q2} and i_{Q4} under the rated power are shown in Figure 8. It is clear that the frequency of i_{Cb} is twice the frequency of i_{Q2} and i_{Q4}. Figure 9 gives the test results of primary voltage and current of full-bridge resonant circuit under the rated power. It can be seen that the higher switching frequency at 52 V input will result in low circulating current compared to at 44 V input.

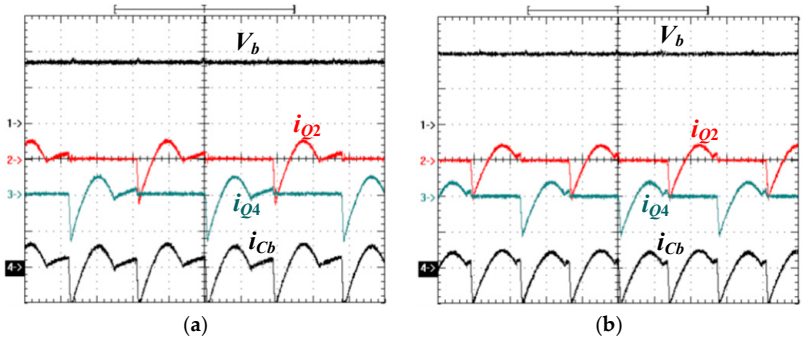

Figure 8. Measured waveforms of V_b, i_{Cb}, i_{Q2} and i_{Q4} under the rated power and (**a**) V_{in} = 44 V (**b**) V_{in} = 52 V [V_b: 50 V/div; i_{Q2}, i_{Q4}, i_{Cb}: 20 A/div; time: 4 μs/div].

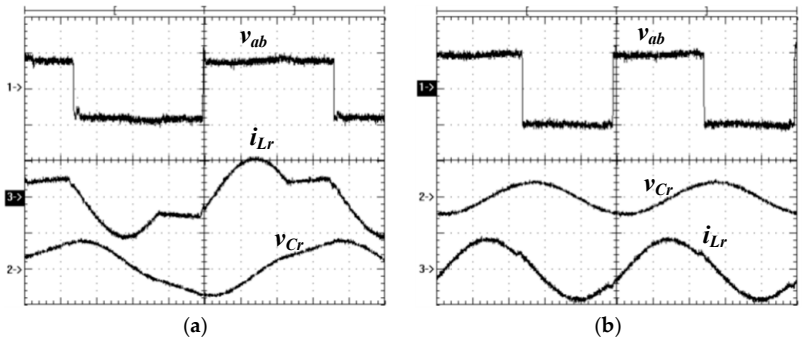

Figure 9. Measured waveforms of v_{ab}, i_{Lr} and v_{Cr} under the rated power and (**a**) 44 V input voltage (**b**) 52 V input voltage [v_{ab}, v_{Cr}: 100 V/div; i_{Lr}: 20 A/div; time: 2 μs/div].

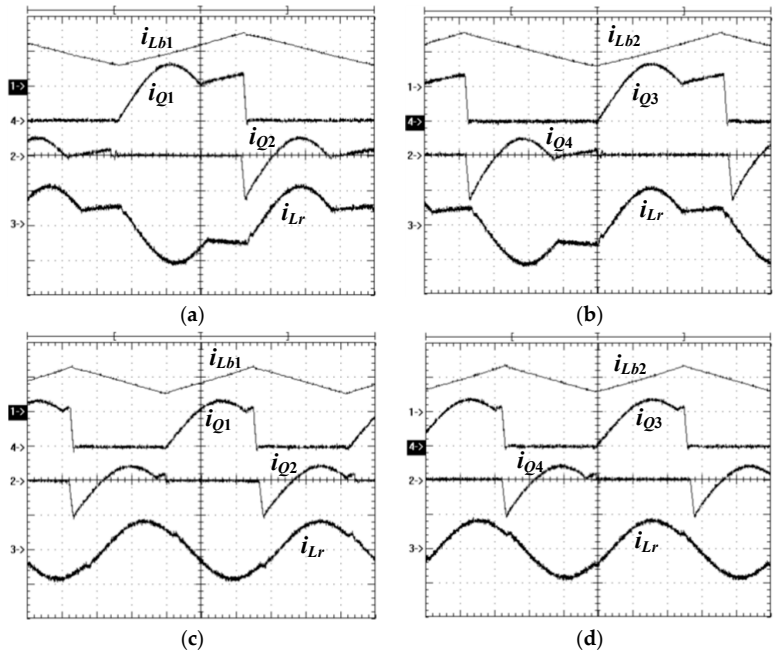

Figure 10. Test results of the switch current and inductor current on the primary side under the rated power (**a**) i_{Lb1}, i_{Q1}, i_{Q2} and i_{Lr} at 44 V input case (**b**) i_{Lb2}, i_{Q3}, i_{Q4} and i_{Lr} at 44 V input case (**c**) i_{Lb1}, i_{Q1}, i_{Q2} and i_{Lr} at 52 V input case (**d**) i_{Lb2}, i_{Q3}, i_{Q4} and i_{Lr} at 52 V input case [i_{Lb1}, i_{Lb2}: 10 A/div; i_{Q1}~i_{Q4}, i_{Lr}: 20 A/div; time: 2 μs/div].

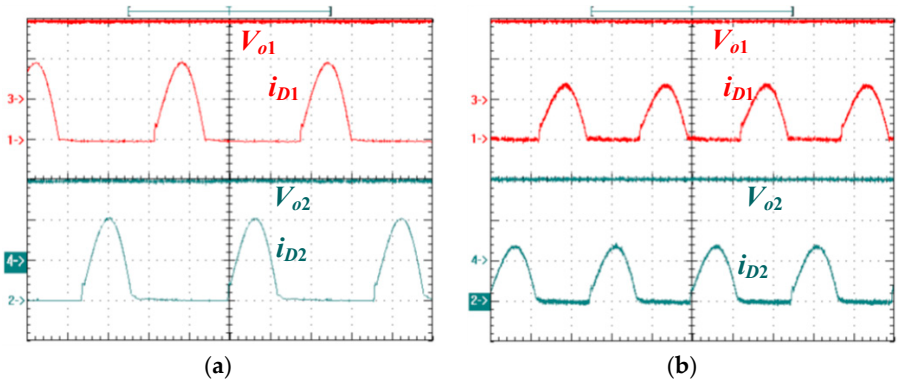

Figure 11. Test results of V_{o1}, V_{o2}, i_{D1} and i_{D2} under the rated power and (**a**) 44 V input case (**b**) V_{in} = 52 V input case [V_{o1}, V_{o2}: 100 V/div; i_{D1}, i_{D2}: 5 A/div; time: 4 µs/div].

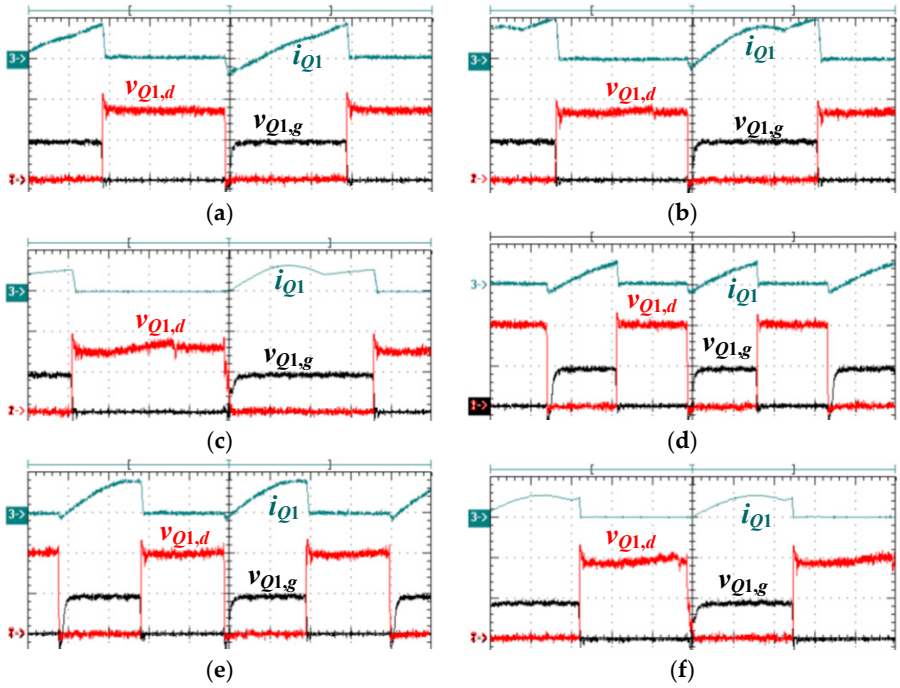

Figure 12. Measured results of switch Q_1 under (**a**) V_{in} = 44 V and 20% load (**b**) V_{in} = 44 V and 50% load (**c**) V_{in} = 44 V and full load (**d**) V_{in} = 52 V and 20% load (**e**) V_{in} = 52 V and 50% load (**f**) V_{in} = 52 V and full load [$v_{Q1,g}$: 10 V/div; $v_{Q1,d}$: 50 V/div; i_{Q1}: 20 A/div for (**a**,**b**,**d**,**e**) and 50 A/div for (**c**,**f**); time: 2 µs/div].

Figure 10 illustrates the test results of i_{Lb1}, i_{Lb2}, i_{Q1}~i_{Q4} and i_{Lr} under the rated power. The peak current of i_{Q1} is larger than the peak current of i_{Q2} due to $i_{Q1} = i_{Lb1} - i_{Lr}$ and $i_{Lr} < 0$ when Q_1 is conducting. The test and experimental results of the output capacitor voltages and rectifier diode currents under the rated power are shown in Figure 11. V_{o1} and V_{o2} are balanced well and D_1 and D_2 are turned off under zero-current switching. Figure 12 illustrates the test results of switch Q_1 at 20%, 50% and 100% loads. It can be observed that zero-voltage switching of switch Q_1 is realized. Since Q_2~Q_4 have the same operation characteristics of Q_1, it can be expected that the zero-voltage switching of switches Q_2~Q_4 are also achieved. The measured efficiencies of the developed converter are 90.5% (at 20% load), 92.6% (at 50% load) and 94.5% (at 100% load) under 52 V input. The measured switching frequencies are 131 kHz (at 20% load), 118 kHz (at 50% load) and 99 kHz (at 100% load) under 52 V input.

6. Conclusions

A novel frequency-controlled current-fed resonant circuit with no input current ripple is proposed and verified in this paper. Theoretical examination and test verification demonstrate that a high-performance resonant circuit with low switching losses and input current ripple-free is achieved with the developed circuit topology. The zero-voltage switching of active devices on the low-voltage side and zero-current switching of rectifier diodes on the high-voltage side are also realized at the whole load range. The test results with the 1 kW laboratory prototype clearly provide the claimed characteristics. The constructed converter can be applied in the renewable energy conversion system with low-voltage input (48 V) and high-voltage output (400 V) with no input current ripple. The studied converter can be used in a battery charger/discharger with switches on the high-voltage terminal in the proposed converter. If the input voltage is from the PV solar cell panel, a slightly wider input voltage variation is expected. Then, the wider switching frequency range and maximum power point tracking must be implemented to regulate the load voltage.

Acknowledgments: This research is supported by the Ministry of Science and Technology, Taiwan, under contract MOST 105-2221-E-224-043-MY2. The authors would also like to thank the anonymous reviewers for their valuable comments and suggestions to improve the quality of the paper.

Author Contributions: Bor-Ren Lin designed the main parts of the project and was also responsible for writing the paper. Guan-Hong Lin built the prototype circuit and measured the experimental waveforms.

Conflicts of Interest: The author declares no potential conflict of interest.

References

1. Wang, J.; Peng, F.Z.; Anderson, J.; Joseph, A.; Buffenbarger, R. Low cost fuel cell converter system for residential power generation. *IEEE Trans. Power Electron.* **2004**, *19*, 1315–1322. [CrossRef]
2. Nymand, M.; Andersen, M.A.E. High-efficiency isolated boost dc–dc converter for high-power low-voltage fuel-cell applications. *IEEE Trans. Ind. Electron.* **2010**, *57*, 505–514. [CrossRef]
3. Zhang, Z.; Thomsen, O.C.; Andersen, M.A.E. Soft-switched dual-input DC–DC converter combining a boost-half-bridge cell and a voltage-fed full-bridge cell. *IEEE Trans. Power Electron.* **2013**, *28*, 4897–4902. [CrossRef]
4. Yuan, Y.; Wu, Q. One zero-voltage-switching three-transistor push–pull converter. *IET Power Electron.* **2013**, *6*, 1270–1278. [CrossRef]
5. Moon, D.; Park, J.; Choi, S. New interleaved current-fed resonant converter with significantly reduced high current side output filter for EV and HEV applications. *IEEE Trans. Power Electron.* **2015**, *30*, 4264–4271. [CrossRef]
6. Prasanna, U.R.; Rathore, A.K. Extended range ZVS active-clamped current-fed full-bridge isolated dc/dc converter for fuel cell applications: Analysis, design and experimental results. *IEEE Trans. Ind. Electron.* **2013**, *60*, 2661–2672.
7. Kim, H.; Yoon, C.; Choi, S. An improved current-fed ZVS isolated boost converter for fuel cell application. *IEEE Trans. Power Electron.* **2001**, *25*, 2357–2364. [CrossRef]
8. Korotkov, S.; Meleshin, V.; Nemchinov, A.; Fraidlin, S. Small-signal modeling of soft-switched asymmetrical half-bridge DC/DC converter. In Proceedings of the IEEE-APEC Conference on Applied Power Electronics Conference and Exposition, Dallas, TX, USA, 5–9 March 1995; Volume 2, pp. 707–711.
9. Tschirhart, D.J.; Jain, P.K. Design procedure for high-frequency operation of the modified series-resonant APWM converter to reduce size and circulating current. *IEEE Trans. Power Electron.* **2012**, *27*, 4181–4191. [CrossRef]
10. Kim, B.C.; Park, K.B.; Moon, G.W. Asymmetric PWM control scheme during hold-up time for LLC resonant converter. *IEEE Trans. Ind. Electron.* **2012**, *59*, 2992–2997. [CrossRef]
11. Mishima, T.; Akamatsu, K.; Nakaoka, M. A high frequency-link secondary-side phase-shifted full-bridge soft-switching PWM DC-DC converter with ZCS active rectifier for EV battery charged. *IEEE Trans. Power Electron.* **2013**, *28*, 5758–5773. [CrossRef]

12. Lin, B.R.; Shiau, T.Y. Zero-voltage switching full-bridge DC/DC converter with parallel-connected output and without output inductor. *IET Power Electron.* **2013**, *6*, 505–515. [CrossRef]
13. Safaee, A.; Jain, P.; Bakhshai, A. A ZVS pulsewidth modulation full-bridge converter with a low RMS current resonant auxiliary circuit. *IEEE Trans. Power Electron.* **2016**, *31*, 4031–4047. [CrossRef]
14. Haga, H.; Kurokawa, F. A novel modulation method of the full bridge three-level LLC resonant converter for battery charger of electrical vehicles. In Proceedings of the IEEE Energy Conversion Congress and Exposition (ECCE), Montreal, QC, Canada, 20–24 September 2015; pp. 5498–5504.
15. Johnson, S.; Erickson, R. Steady-state analysis and design of the parallel resonant converter. *IEEE Trans. Power Electron.* **1988**, *3*, 93–104. [CrossRef]
16. Gu, Y.; Lu, Z.; Hang, L.; Qian, Z.; Huang, G. Three-level LLC series resonant DC/DC converter. *IEEE Trans. Power Electron.* **2005**, *20*, 781–789. [CrossRef]
17. Steigerwald, R.L. A comparison of half-bridge resonant converter topologies. *IEEE Trans. Power Electron.* **1988**, *3*, 174–182. [CrossRef]